https://doi.org/10.5194/egusphere-2023-1603
Preprint. Discussion started: 18 July 2023

Short summary. 250 m estimates of snow in the Western US and Canada were improved by assimilating observations representative of a future snow-focused satellite mission with a land surface model. Here, by including a gap-filling strategy, snow estimates could be improved in forested regions where remote sensing is challenging. This approach improved estimates of winter maximum snow water volume to within 4%, on average, with persistent improvements to both snow and runoff throughout spring snowmelt.

Extending the utility of space-borne snow water equivalent observations over vegetated areas with data assimilation

Justin M. Pflug[1,2], Melissa L. Wrzesien[1,2], Sujay V. Kumar[2], Eunsang Cho[1,2], Kristi R. Arsenault[3,2], Paul R. Houser[4], Carrie M. Vuyovich[2]

[1]Earth System Science Interdisciplinary Center, University of Maryland, College Park, MD, USA
[2]Hydrological Sciences Laboratory, NASA Goddard Space Flight Center, Greenbelt, MD, USA
[3]Science Applications International Corporation, McLean, VA, USA
[4]Geography and Geoinformation Science Department, George Mason University, Fairfax,VA, USA

Correspondence to: Justin Pflug (Justin.Pflug@nasa.gov)

Abstract. Snow is a vital component of the Earth system. Yet, no snow-focused satellite remote sensing platform currently exists. In this study, we investigate how synthetic observations of snow water equivalent (SWE) representative of a synthetic aperture radar remote sensing platform could improve spatiotemporal estimates of snowpack. We use an Observation System Simulation Experiment, specifically investigating how much snow simulated using popular models and forcing data could be improved by assimilating synthetic observations of SWE. We focus this study across a 24°-by-37° domain in the Western United States and Canada, simulating snow at 250 m resolution and hourly timesteps in water-year 2019. We perform two data assimilation experiments, including: 1) a simulation excluding synthetic observations in forests where canopies obstruct remote sensing retrievals, and 2) a simulation inferring snow distribution in forested grid cells using synthetic observations from nearby canopy-free grid cells. Results found that assimilating synthetic SWE observations improved average SWE biases at peak snowpack timing in shrub, grass, crop, bare-ground, and wetland land cover types from 14%, to within 1%. However, forested grid cells contained a disproportionate amount of SWE volume. In forests, SWE mean absolute errors at peak snowpack were 111 mm, and average SWE biases were on the order of 150%. Here, the data assimilation approach that estimated forest SWE using observations from the nearest canopy-free grid cells substantially improved these SWE biases (18%) and the SWE mean absolute error (27 mm). Simulations employing data assimilation also improved estimates of the temporal evolution of both SWE and runoff, even in spring snowmelt periods when melting snow and high snow liquid water content prevented synthetic SWE retrievals. In fact, in the Upper Colorado River basin, melt-season SWE biases were improved from 63% to within 1%, and the Nash Sutcliffe Efficiency of runoff improved from –2.59 to 0.22. These results demonstrate the value of data

https://doi.org/10.5194/egusphere-2023-1603
Preprint. Discussion started: 18 July 2023

assimilation and a snow-focused globally relevant remote sensing platform for improving the characterization of SWE and associated water availability.

1 Introduction

Snow plays important roles in the Earth system, by regulating global temperatures and cooling the land surface because of its reflective properties (Barry, 2002). The insulative properties of snow are also vital in ecological balance by protecting plants and animals from extreme cold and providing moisture when it melts. Snow is a major source of water storage for many regions, especially in areas that rely on snowpack to sustain water resources during the dry season. It has been estimated that more than 2 billion people around the world are reliant on seasonal snow melt for their water supply (Barnett et al., 2005). Snowpack is the natural 'integrator' of climatic conditions and offers more predictability of water availability than variables with shorter memory, such as precipitation and streamflow (Terzago et al., 2023). As a result, accurate wintertime estimates of snowpack are critical for water management and agricultural planning (Koster et al., 2010). Water managers can prepare mitigation strategies for extreme dry or wet possibilities based on the wintertime snowpack. For example, in the Western U.S., where a vast majority streamflow originates from snow (Li et al., 2017), it is common practice to use the April 1 snowpack, the historic peak for snowpack in that region, for developing water supply estimates for later in the season. However, climate change impacts have led to increased variability in the snow seasonality (Livneh and Badger, 2020), with warmer temperatures reducing the amount of snow accumulation and seasonal snow storage, and advancing the timing of the spring melt. Therefore, accurate characterization of winter snowpack and its variability is critically important for making informed water supply quantifications.

In recognition of the critical need to have spatially distributed measurements of snow mass, there have been several efforts to measure snowpack and snow water equivalent from many different remote sensing platforms in the past several decades. Airborne lidar systems have been able to provide high resolution, accurate measurements of snow mass (Painter et al., 2016), but this approach has significant logistical barriers for global and frequent snow measurements, and the hydrological utility of a practical spaceborne lidar platform is limited (Kwon et al., 2021). In the past three decades, snow depth and SWE estimates have been derived from passive microwave remote sensing measurements, but they tend to be of coarse spatial resolution, and have limited accuracies over deep snow, complex terrain, and dense vegetation (REF). Active microwave remote sensing instruments such as Synthetic Aperture Radars (SARs) can provide finer spatial resolution measurements, and have shown promise in obtaining high quality observations in deep snow environments (Lievens et al., 2019). While these instruments can observe in night-time and cloudy conditions, they are still limited over areas with dense vegetation (Tsang et al., 2022). Further, all spaceborne instruments have inherent coverage gaps due to their orbital and revisit configurations.

To overcome these limitations, modeling and data assimilation systems are needed that can extend the coverage and utility of available measurements to areas, times, and variables that are not directly observed. In this article, we present a novel

https://doi.org/10.5194/egusphere-2023-1603
Preprint. Discussion started: 18 July 2023

approach through data assimilation, designed specifically to improve the usefulness of spaceborne SWE retrievals over forested areas. The approach is demonstrated using an observing system simulation experiment (OSSE; e.g., Cho et al., 2022; Errico et al., 2007) which is an approach used to formally assess the impact of the data to be collected from an anticipated mission. Several prior studies have examined the use of OSSEs for snow mission studies (Garnaud et al., 2019; Kwon et al., 2021; Wrzesien et al., 2022). Among them, SAR-focused OSSEs have been conducted by Garnaud et al. (2019) and Cho et al. (2022) to assess the utility of hypothetical snow observations. Garnaud et al. (2019) focused on a Ku-band SAR to quantify trade-offs between sensor configurations (e.g., various spatial resolutions and revisit frequencies) with retrieval algorithm accuracy and SWE performance in southern Quebec, Canada, where temperate forests are dominant with shallow and moderate snowpack conditions. Cho et al. (2022) conducted a X-/Ku-band SAR OSSE with an achievable sensor configuration (1 km spatial resolution, 7-day revisit frequency, and orbital configurations using the Trade-space Analysis Tool for Constellations [TAT-C] simulator) focusing on mountainous environments in a western Colorado. To comprise diverse snow environments, specifically for various forested landscapes in this study, we focus on developing an OSSE covering the entire western United States domain along with the proposed, more realistic constellations using TAT-C. We simulate finer-scale (250 m) synthetic SWE observations that could be provided from a future SAR mission, which are then incorporated within a land surface model through data assimilation to assess their capability to improve snow state estimates, and the integrated impact on hydrologic states in space and time. The assimilation experiments here are conducted with and without a novel strategy to extend SAR-based observational coverage of snow mass to various forested landscapes.

The primary contribution of this paper is the development of a viable strategy for extending space borne remote sensing SWE measurements in preparation of a future snow mission concept (a volume-scattering X-/Ku band SAR). We specifically focus on addressing the following research questions: 1) what is the added utility of spaceborne active remote sensing SWE retrievals across the western United States? 2) how much can spatiotemporal representations of SWE be improved by focusing on developing observationally based snow estimates over areas with dense vegetation, where SAR sensors may be limited? 3) How much added hydrological utility can be obtained through spaceborne active remote sensing measurements and data assimilation approaches, particularly when coverage over forested areas is improved?

Section 2 describes the study domain and OSSE modeling setup. This is followed by the description of the results (Sect. 3), a discussion of the findings (Sect. 4), and the study's conclusions (Sect. 5).

2.1 Study domain and OSSE setup

As noted above, an OSSE is a typical approach used to assess the value of the data to be collected from an anticipated mission, and consists of the following steps: 1) Development of an assumed "true state" of the relevant system is produced by a "nature run" that involves the use of a state-of-the-art model employed with the best available boundary conditions (Sect. 2.1); 2) simulation of synthetic observations from the nature run, accounting for sources of sensing limitations, sensing

https://doi.org/10.5194/egusphere-2023-1603
Preprint. Discussion started: 18 July 2023

uncertainties, and orbital configurations (Sect. 2.2); 3) incorporation of the simulated observations (often through data assimilation, Sect. 2.3) in a different, model configuration with accuracies representative of common modeling biases and uncertainties, often called the 'open loop'; and 4) evaluation of the impact that the simulated data have on improving the performance relative to the nature run. The details of the OSSE setup used in this manuscript, are described below, including a novel approach for inferring SWE in forested landscapes from nearby, unforested simulated observations (Sect. 2.4).

We employ the NASA Land Information System (LIS; Kumar et al., 2006), an infrastructure for high performance, ensemble-based land surface modelling and data assimilation to enable this OSSE. LIS encompasses several advanced land surface models that can simulate terrestrial water, energy, and carbon balances and related states such as soil moisture, land surface temperature, and SWE, among others. These include different versions of community models such as Noah (Ek et al., 2003), Variable Infiltration Capacity (VIC; Liang et al., 1994), Catchment (Koster et al., 2000), Joint UK Land Environment Simulator (JULES; Best et al., 2011), and Noah-MP (Niu et al., 2011). The LIS framework also includes support for specialized models that are designed to provide more detailed representations of certain land surface processes (e.g. snow), while enabling interaction with LSMs that solve for water, energy, and carbon balances at a macroscale. For example, the advanced snow physics model called SnowModel (Liston and Elder, 2006) has been incorporated within LIS in a manner that allows coupling to existing LSMs. This structure allows the use of the advanced snow physics from SnowModel while leveraging the existing process schemes (e.g., sub-surface, groundwater, canopy) within the LSMs. Here we utilize these unique capabilities for enabling the OSSE integrations.

The study is conducted over a large domain (Fig. 1), covering the Western U.S. from 31-55N and 93-130W at a 250 m spatial resolution. As shown in Fig. 1, this modeling domain encompasses a broad range of vegetation types, topographical regimes and river basins of the Pacific Northwest, California, Great Basin, and Upper Colorado. 22% of the domain is covered by forests, with grasslands, croplands, and shrublands accounting for 20%, 23%, and 26% of the domain, respectively. Forests dominate the coverage of areas with significant snowpack, occupying 58% of regions that are in the mid-elevation range of 2500-3500m, and 15% of the areas with elevations over 3500m. From a modelling perspective, the domain extent of Fig. 1 (~83 million land grid points) is computationally challenging. The scalable high performance computational and parallel inputting and outputting capabilities of NASA LIS were leveraged to enable these simulations. A multiprocessor configuration involving approximately 1000 processors was employed to facilitate large model simulations for the nature run, open loop simulation, and two simulations with data assimilation.

https://doi.org/10.5194/egusphere-2023-1603
Preprint. Discussion started: 18 July 2023

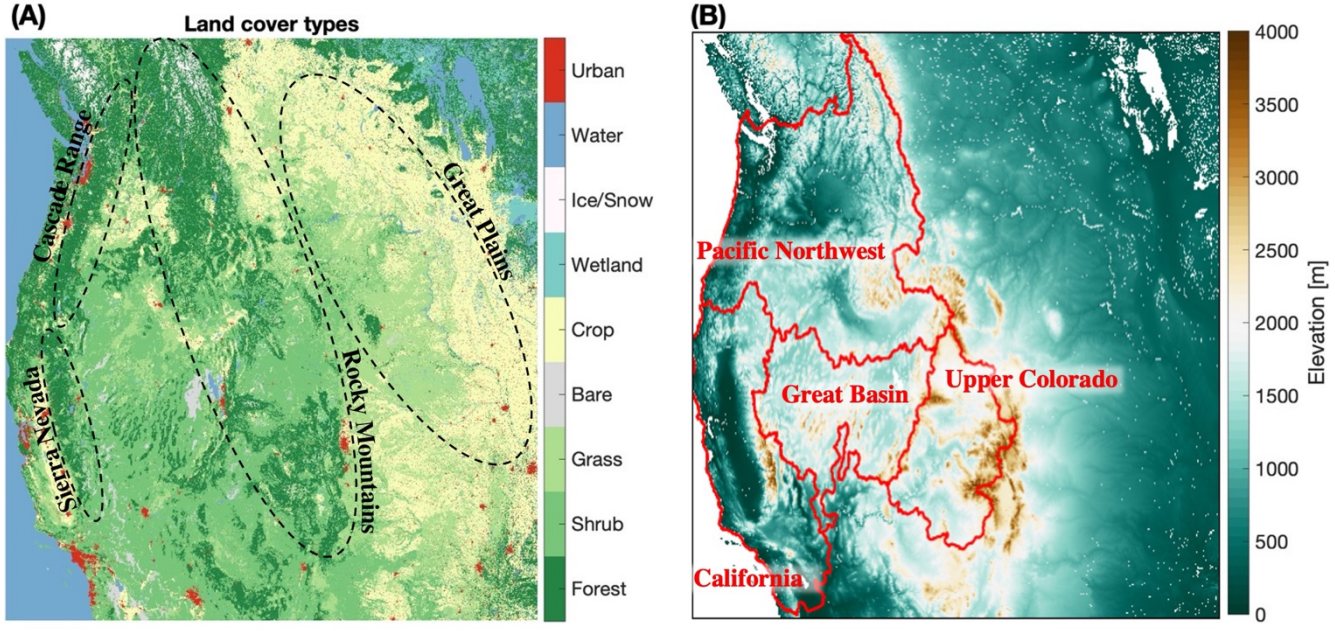

Figure 1: Maps of the land and vegetation classes (A; left panel) and elevation (in meters) (B; right panel) used in the simulations. Outlines and labels in the left panel indicate regions discussed in the Results (Sect. 4). Red contours in the right panel indicate basins used in the analysis.

The "nature run" in this study was performed using a model configuration that coupled a state-of-the-art and physically based snow model (named SnowModel, discussed later in this section) with the Noah model with multi-parameterization (Noah-MP) version 4.0.1. The simulations are conducted by forcing this coupled model setup with the surface meteorology from NASA's Modern Era Retrospective Reanalysis, version 2 (MERRA2; Gelaro et al., 2017) product, with LIS-provided downscaling to 250 m resolution using lapse rates and topographical downscaling approaches, like SW corrections based on topographical shading (Arsenault et al., 2018). The model integrations were conducted for the water year 2019 (September 2018 – September 2019), which was a wetter than normal year based on the long-term average meteorological conditions over this domain. The open loop and data assimilation integrations performed in this study were conducted using Noah-MP alone.

The Noah-MP model discussed above evolved from the Noah LSM, with multiple options for various land surface processes. It represents processes related to energy, water, and carbon balances at the land surface by accounting for processes related to infiltration, evaporation, transpiration, runoff generation and groundwater recharge. A TOPMODEL-based runoff model is used to calculate surface runoff and groundwater discharge. Options for prognostic vegetation dynamics models that represent the growth and senescence of vegetation are also available within Noah-MP. A two-stream radiative transfer approach is employed to calculate surface energy processes. A multilayer snowpack model (with up to three layers) that can account for snow melt metamorphisms, compaction by overlying snow, sublimation of canopy intercepted snow, and snowmelt-refreeze cycles is available within Noah-MP (Niu and Yang, 2004).

https://doi.org/10.5194/egusphere-2023-1603
Preprint. Discussion started: 18 July 2023

Snow states like snow depth and SWE were also modelled across the Western United States (domain highlighted in Fig. 1) at 250 m resolution and hourly time steps using the single-layer implementation of SnowModel (Liston and Elder, 2006). This model has seen widespread use in the snow community, demonstrating the capability to resolve snow evolution in a variety of landscapes and complex snow processes like the redistribution of snow via wind, and the resulting impact on snow distribution, melt season snow duration, glacier mass balance, and snow habitat for species like polar bears and Dall sheep (Hiemstra et al., 2002; Liston et al., 2016; Mahoney et al., 2018; Mernild et al., 2017; Sturm and Wagner, 2010). Snow evolution at each grid cell accounted for a wide set of snow processes, including snow sublimation, snow grain size evolution, solar topographical shading, canopy shading, canopy snow interception, and wind redistribution. Through the coupling, Noah-MP snow states and the resulting snow-driven runoff were updated using the SnowModel outputs at daily timesteps for each grid cell. Preliminary research has shown that relative to Noah-MP, LIS simulations coupling Noah-MP with SnowModel have improved the volume and spatial distribution of simulated snow depth and SWE (Wrzesien et al., 2022). Therefore, the coupled SnowModel and Noah-MP model was a prime candidate for the "nature run" in this study, or the simulation most representative of the true underlying spatiotemporal snow states from which simulated observations were derived (Sect. 2.2), and the assimilated model was compared against.

2.2 Observation simulator

From the nature run integrations conducted with Noah-MP coupled to SnowModel in LIS, synthetic SWE retrievals at 250 m spatial resolution, expected from a hypothetical SAR mission, were simulated. First, the orbital swaths were simulated using TAT-C (Le Moigne et al., 2017). TAT-C, a NASA software system designed for future Distribution Spacecraft Missions (DSM), enables us to explore a range of feasible design options (e.g., constellation vs. single, geostationary vs. polar-orbiting, low vs. high temporal frequencies) to estimate optimal gains for the given mission configuration. Using an assumed 10-14 day revisit frequency, these orbital swaths were applied to the nature run outputs to simulate the satellite viewing area. The realistic spatial coverage is simulated by extending the ground track to a swath width (i.e., 50 km). The daily viewing extents are simulated as a daily binary map (so-called "cookie cutter") masking the surface as viewed or not at a 250 m spatial resolution. Additionally, based on an error level of 20%, spatially and temporally uncorrelated random errors drawn from a Gaussian distribution were added to the synthetic SWE retrievals. Note that here we use an optimistic assumption of uniform error levels throughout the domain, whereas in reality, the errors are likely to be dependent on other factors, including the terrain characteristics, vegetation, and precipitation regime.

2.3 Data assimilation setup

A one-dimensional ensemble Kalman Filter (EnKF; Reichle et al., 2002) was used to assimilate the synthetic observations within the open loop configuration of the model. EnKF is widely used for land data assimilation studies (Kumar et al., 2022), as it provides a flexible approach for the treatment of model and observation errors and non-linear models. An ensemble of model realizations is used by EnKF to assess and propagate model errors. In this instance, the ensemble requirement further

https://doi.org/10.5194/egusphere-2023-1603
Preprint. Discussion started: 18 July 2023

adds to the significant computational requirements of the large model domain (Fig. 1) and fine spatial resolution of the simulations (250 m). Therefore, a 5-member ensemble with perturbations applied to the meteorological variables and model prognostic fields are used for simulating uncertainty in the modelled estimates. Table 1 details the parameters for meteorological and model state perturbations, which are based on recent snow data assimilation studies (Lahmers et al., 2022; Kwon et al., 2021). Though a larger ensemble size is better for ensuring sufficient sampling density, our choice of five ensembles is reasonable given that the model state vector used in the assimilation only consists of two variables; the total SWE and snow depth. The assimilation setup employs a sequential update strategy, where at each time step an ensemble of model forecasts is propagated forward in time, followed by an update based on observational inputs. The model states are updated toward the observations based on the relative uncertainties in the model and observations using the following formulation, at a certain time k.

$$x_k^{i+} = x_k^{i-} + K_k\left[y_k^i - H_k x_k^{i-}\right] \quad \text{Eq. (1)}$$

Where x_k and y_k are the model and observation state vectors, respectively. The term H_k represents the observation operator that maps the model states to the observed variables. The superscripts $i-$ and $i+$ represent the ith ensemble member before and after the update, respectively. K_k is the "Kalman gain" term, that allows the weighting of the observations and model forecasts is a function of the model and observation error covariances.

https://doi.org/10.5194/egusphere-2023-1603
Preprint. Discussion started: 18 July 2023

Table 1. Model forcing and state-variable perturbations used by the 5-member ensemble of LIS simulations

Variable	Perturbation Type	Std. Dev.	Cross Correlation across variables			
Meteorological Forcing			SW corr	LW corr	PCP corr	T corr
Downward Shortwave (SW)	Multiplicative	0.2	1	−0.3	−0.5	0.3
Downward Longwave (LW)	Additive	30	−0.3	1	0.5	0.6
Precipitation (PCP)	Multiplicative	0.5	−0.5	0.5	1	−0.1
Near surface Air Temperature (T)	Additive	0.5	0.3	0.6	−0.1	1
Noah-MP LSM snow states			SWE	Snow depth		
SWE	Multiplicative	0.01	1	0.9		
Snow depth	Multiplicative	0.01	0.9	1		

The data assimilation procedure detailed here assimilated the synthetic SWE retrievals (Sect. 2.2) with the open loop simulation. The degree to which the simulation with data assimilation approached SWE simulated by the nature run is intended to represent the extent to which a SAR remote sensing platform with the SWE retrieval characteristics from Sect. 2.2 could be combined with a land surface model to provide near real-time estimates of SWE at 250 m resolution. However, the SAR observations synthesized in this study have known issues with observing snow with high liquid water contents and dense forest cover. Therefore, synthetic observations at each timestep were masked at grid cells with deciduous, evergreen, and mixed forest cover (Fig. 1), and at grid cells where and when snow was experiencing melt. Although limited in area, grid cells with "ice" landcover (Fig. 1) were also excluded. In Sect. 2.4 below, we present a novel approach used to infer SWE in grid cells with forests using the nearest canopy-free synthetic observations.

2.4 Extending observations over forests

The 1-d EnKF approach employed here updated each model grid SWE from the open loop simulation based on the observations available at that grid point. Though studies have employed 3-d EnKF approaches to spatially propagate observational information to neighbouring grid cells (De Lannoy et al., 2012) , here we relied on 1-d updates due to several factors. First, a 2-d update requires the knowledge of spatial error correlations and their variability, which is challenging to

https://doi.org/10.5194/egusphere-2023-1603
Preprint. Discussion started: 18 July 2023

specify (Ying, 2020). Most prior studies using such schemes employ uniform specifications and are limited to small domains. Second, a 2-d update increases the size of the state vector and consequently requires the use of a larger ensemble. This, combined with the added computational expense of a 2-d analysis significantly increases the computational cost. Therefore, we employed an alternate approach that is computationally more efficient while allowing the extension of observations to nearby areas.

Assuming that the SWE retrievals from the hypothetical SAR instrument are limited over forested areas, here we employ a novel approach to extend the observations obtained in non-forested areas (Fig 2). For every forested location, valid retrievals over nearby non-forested locations within a radius of influence of 750 m are identified. An observation at the forested pixel is then estimated by scaling the model SWE by the ratio of the average observed SWE to modeled SWE over the 'clearing' areas (Fig. 2). This scaled observation is then used for assimilation over the forested pixel. Here we implicitly use the spatial correlations inherent in the model between forested and clearing areas to extend observational coverage over the clearing to forested locations. To evaluate the accuracy and added value of this scaling approach, we compare SWE and runoff from the nature run simulation, versus simulations with data assimilation both 1) employing the forest scaling strategy discussed here, and 2) masking synthetic observations in forested grid cells (Sect. 2.3).

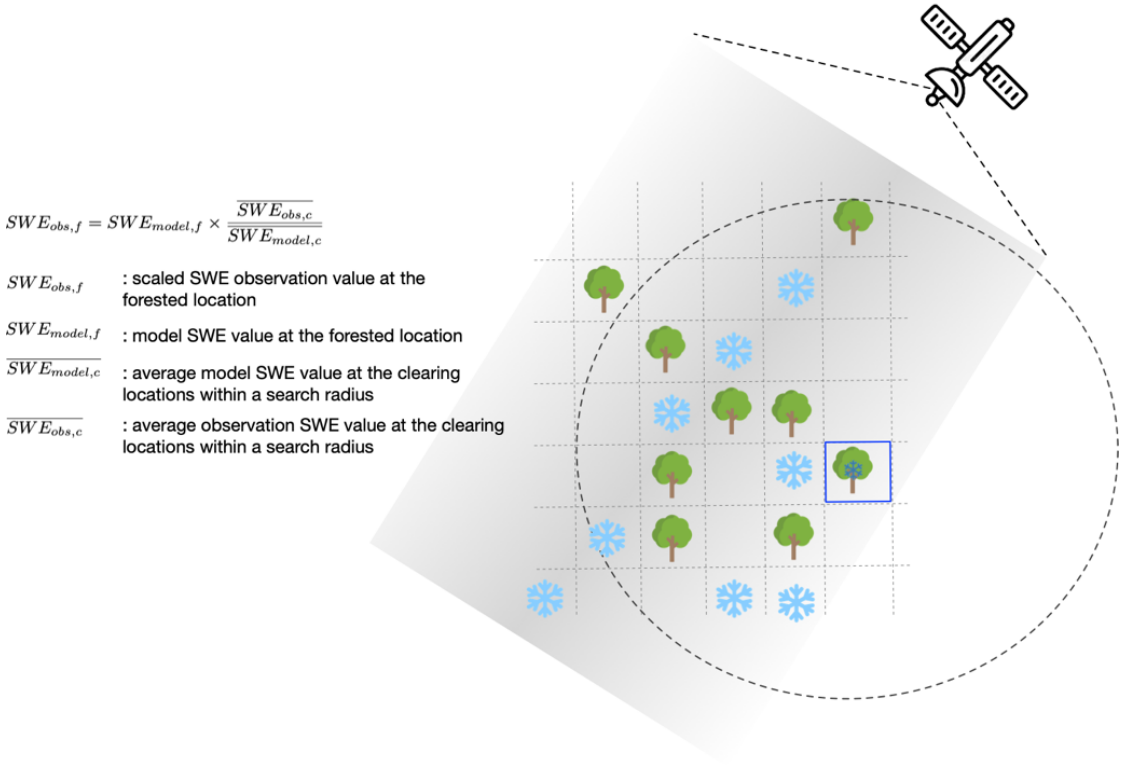

Figure 2. Conceptual depiction and equations demonstrating the forest strategy used here, which estimates a SWE observation at a given grid cell (outlined box in blue color) based on the modeled SWE ($SWE_{model,f}$) and the ratio between the average

https://doi.org/10.5194/egusphere-2023-1603
Preprint. Discussion started: 18 July 2023

synthetic SWE observations ($\overline{SWE_{obs,c}}$) and average modeled SWE ($\overline{SWE_{model,c}}$) from a 750 m radius (dashed circle). The light gray shading represents the satellite swath, the tree icons indicate forested locations, and the snowflake icons represent SWE measurements at non-forested locations.

3 Results

In this section, we compute the difference between the open loop simulation, nature run, and the two simulations with data assimilation, one masking synthetic observations over regions with forests, and the other extending snow estimates in forested regions using the strategy from Sect. 2.4 and Fig. 2. We focus on the differences between these four simulations using: 1) average SWE from the winter snow accumulation season (December, January, and February; DJF), when snowmelt is minimized and synthetic observations are masked by grid cells with liquid water content to the smallest degree, 2) spatially distributed SWE on 13 March, the date corresponding to the timing of maximum SWE volume in water-year 2019, and 3) daily average SWE and total runoff for each day in water-year 2019 over a number of selected river basins including the Pacific Northwest, California, Great Basin, and Upper Colorado (Fig. 1b).

The open loop and nature run simulations exhibited differences in both the volume and spatial distribution of average winter (December, January, and February; DJF) SWE (Fig. 3a and 3b). Relative to the nature run, the open loop simulation tended to simulate lower elevation winter SWE that was both larger in magnitude and persisted for longer before melting. In the Pacific Northwest domain (Fig. 4), DJF average snow cover (defined as grid cells with mean DJF SWE exceeding 5 mm), was approximately 12% larger for the open loop simulation than the nature run (Table 2). These snow extent biases were also apparent in the other basins (Figs. S1 – S3), where open loop snow extents exceeded snow extents from the nature run by 26% in the Upper Colorado, 45% in the Great Basin, and 6% in California. Visually, the nature run had significant increases in the spatial variability of winter SWE, better representing the differences in SWE between mountain peaks and valleys, and the patchiness of snow cover in regions with winter snowmelt and ephemeral snow cover (e.g., Fig. 4). Relative to the nature run, DJF SWE from the open loop simulation was biased high across the full modeling region (Fig. 3) by approximately 26%, on average, with a mean absolute error of 41 mm and spatial coefficient of correlation of approximately 0.74. Across snowy the Pacific Northwest basin (Fig. 4), DJF mean SWE biases were approximately 37%, with a mean absolute error of 55 mm. Open loop model performance for the other basins can be found in Table 2.

https://doi.org/10.5194/egusphere-2023-1603
Preprint. Discussion started: 18 July 2023

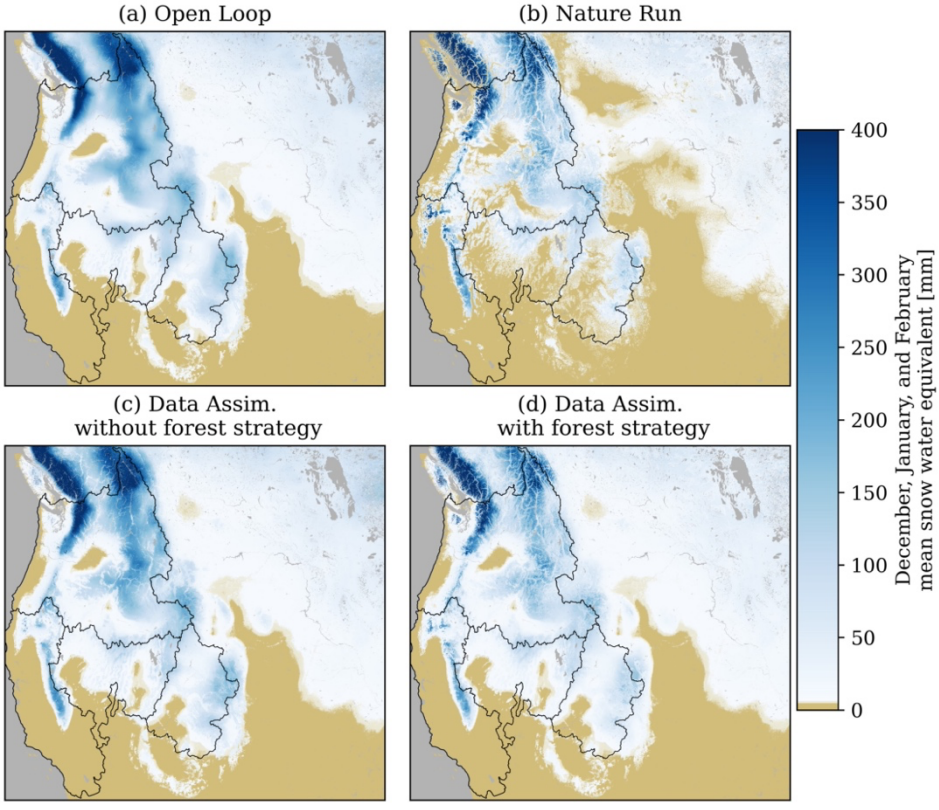

Figure 3. Winter (December, January, and February) mean SWE simulated at 250 m resolution from the open loop (a), nature run (b), and data assimilation simulations, both with (d) and without (c) the forest strategy presented in Sect. 2.4.

https://doi.org/10.5194/egusphere-2023-1603
Preprint. Discussion started: 18 July 2023

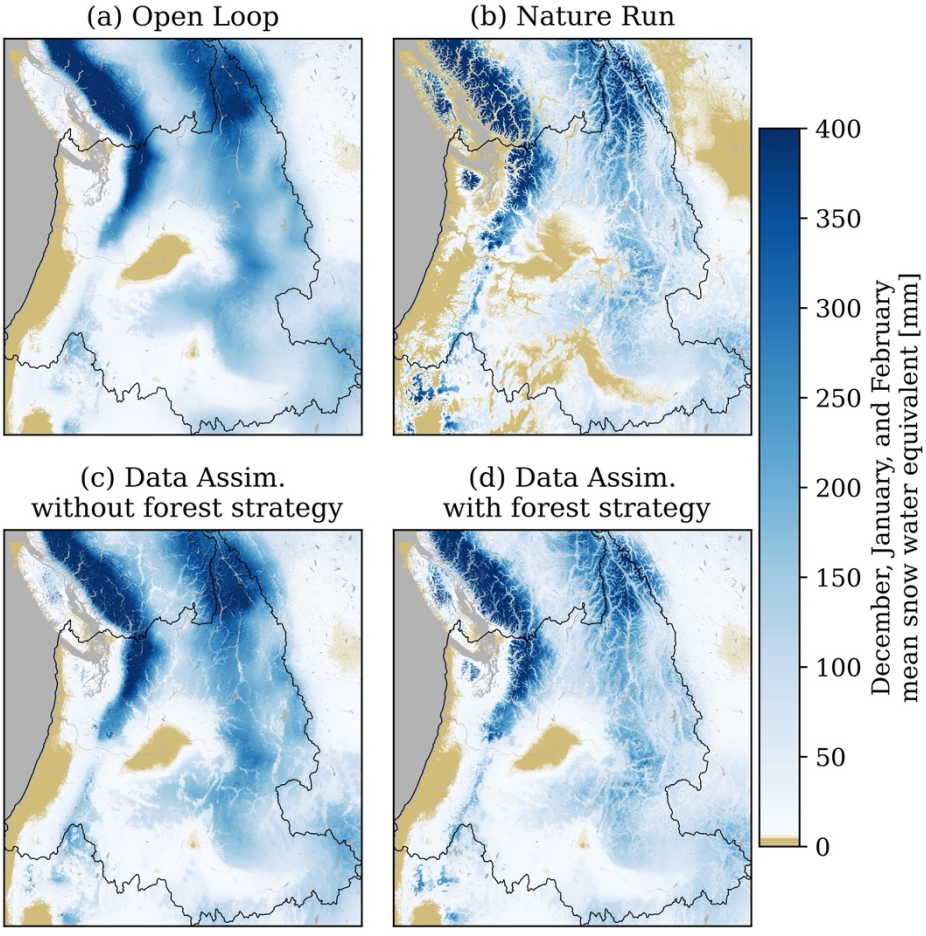

Figure 4. Winter (December, January, and February) mean SWE in the Pacific Northwest region simulated at 250 m resolution from the open loop (a), nature run (b), and data assimilation simulations, both with (d) and without (c) the forest strategy.

https://doi.org/10.5194/egusphere-2023-1603
Preprint. Discussion started: 18 July 2023

Table 2. Simulation performance, relative to the nature run simulation, for the open loop simulation (OL) and the simulations with data assimilation, both with (DA+F) and without (DA) the forest strategy. Statistics are presented for the full domain, the four hydrologic basins, and all forested and unforested grid cells.

		DJF* snow-extent biases	13 March 2019 SWE			Seasonal SWE and runoff	
			Mean bias	SWE abs. error [mm]	Coeff. of corr.	MAM* mean SWE bias	Nash-Sutcliffe Efficiency
Full study domain	OL^	+22%	+26%	41	0.74	-	-
	DA^	+23%	+9%	36	0.79	-	-
	DA+F^	+22%	+4%	17	0.91	-	-
Upper Colorado	OL	+26%	+37%	55	0.74	+63%	-2.59
	DA	+28%	+27%	50	0.74	+86%	-3.71
	DA+F	+28%	+8%	23	0.90	< 1%	0.22
Pacific Northwest	OL	+12%	+42%	89	0.69	+44%	-0.17
	DA	+13%	+32%	80	0.74	+80%	-0.34
	DA+F	+13%	+6%	35	0.89	+15%	0.39
Great Basin	OL	+45%	+35%	38	0.62	-29%	0.58
	DA	+46%	+46%	32	0.75	+10%	0.58
	DA+F	+46%	+28%	23	0.83	-38%	0.53
California	OL	+6%	-34%	50	0.64	-50%	0.92
	DA	+8%	-6%	40	0.79	-15%	0.88
	DA+F	+8%	-6%	28	0.88	-26%	0.89
Unforested	OL	+19%	+14%	22	0.83	-	-
	DA	+20%	< 1%	14	0.91	-	-
	DA+F	+20%	< 1%	14	0.91	-	-
Forested	OL	+29%	+150%	111	0.67	-	-
	DA	+30%	+150%	111	0.67	-	-
	DA+F	+30%	+18%	27	0.93	-	-

* DJF = December, January, and February; MAM = March, April, and May (averages)
^ OL = open loop simulation; DA = simulation with data assimilation; DA+F = simulation with data assimilation and the forest strategy

As expected, the simulations assimilating the synthetic SWE observations agreed with the nature run better than the open loop simulation. However, on 13 March 2019 (the date of maximum domain SWE volume), the simulation with data assimilation without the forest strategy had high-biased SWE across large portions of the Rocky Mountains and the Cascade Mountain range (Fig. 1, Fig. 5b and Fig. 5e). Low biased SWE was more common in Northernmost Canadian portions of the Rocky Mountains and Cascade Range, the Western montane regions in Washington State, the Northern portions of the Great Basin, and the lower-lying elevations of the California Sierra Nevada. Additionally, despite the assimilation, snow extents were still biased high relative to the nature run (Fig. 3) at magnitudes similar to the open loop simulation (Table 2). This was driven by the expansive snow extents of the open loop simulation, which were decreased by data assimilation, but still resulted in widespread early-season SWE increases for short periods of time between synthetic observations (at 10 – 14 day

https://doi.org/10.5194/egusphere-2023-1603
Preprint. Discussion started: 18 July 2023

frequencies), increasing to the number of grid cells with DJF SWE exceeding 5 mm (threshold used to define average winter snow extents in Fig. 3).

Assimilating the synthetic SAR observations without the forest strategy best improved SWE in shrub, grass, crop, bare, and wetland landcover types (Fig. 6b and 6c). For example, relative to the open loop simulation (Fig. 5a and 5d), data assimilation without the forest strategy (Fig. 5b and 5e) corrected the high SWE biases in the Great Plains (Fig. 1). While 13 March SWE in shrub, grass, crop, bare-ground, and wetland regions was typically small in magnitude, these landcover types accounted for 77% of the modeling domain area, and 61% of the domain total SWE volume on 13 March (Fig. 6a). In these regions, SWE from the open loop simulation had a mean absolute error of 22 mm, and a mean bias of approximately 14%, relative to the nature run (Table 2). Data assimilation significantly improved the SWE bias in these land cover types to within 1%, on average (Fig. 6b), with a mean absolute error of 14 mm.

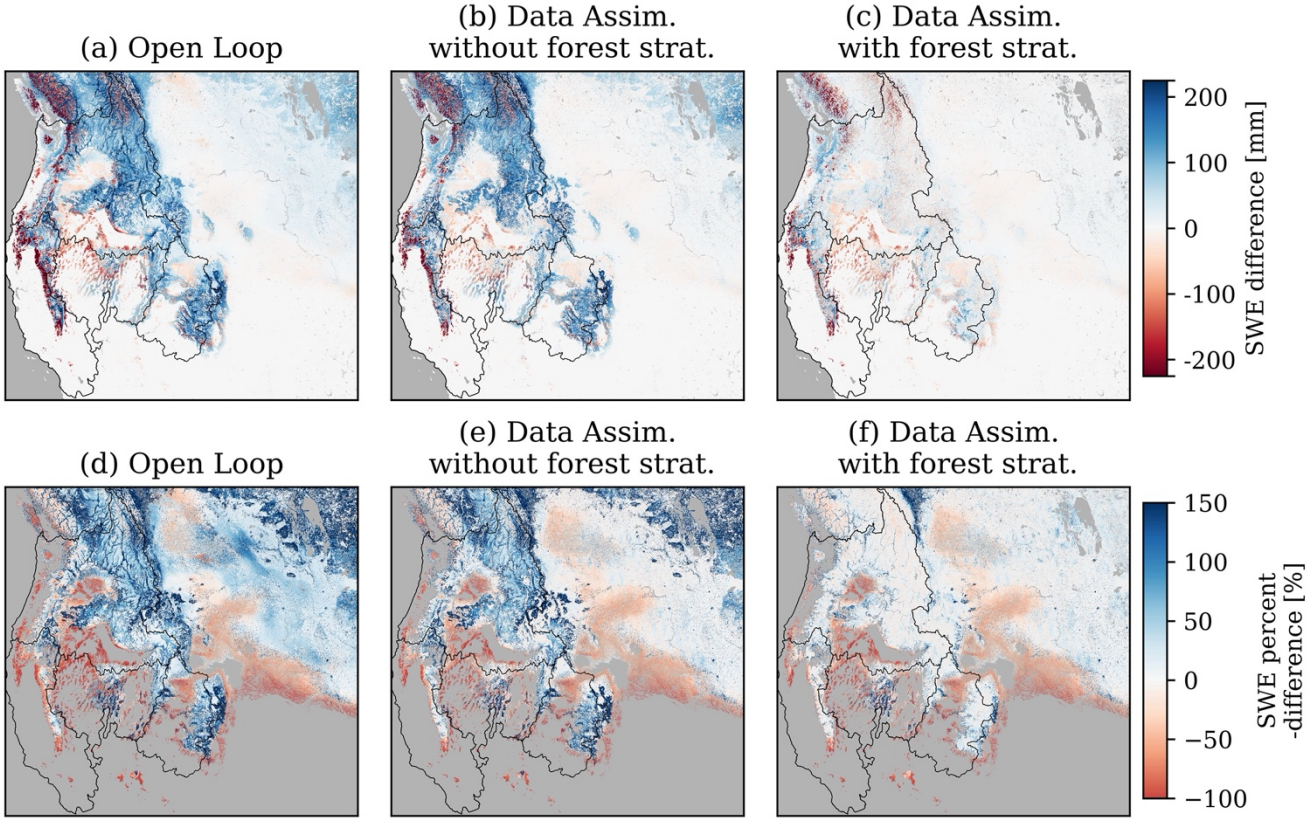

Figure 5. 13 March 2019 SWE difference (top row) and percent-difference (bottom row), relative to the nature run, for the open loop simulation (a and d), and simulations with data assimilation, both with (c and f) and without (b and e) the forest strategy. SWE percent-different maps (bottom row) only compare grid cells where SWE from the nature run was greater than 5 mm.

https://doi.org/10.5194/egusphere-2023-1603
Preprint. Discussion started: 18 July 2023

The data assimilation results discussed above did not use the synthetic observations over forested grid cells, where retrievals from SAR instruments may be either partially or fully occluded by the canopy overstory (Tsang et al., 2022; Ruiz et al., 2022; Huang et al., 2019). However, a significant portion of the snow volume in mid-latitude domains overlaps with forests. For example, although forests only covered approximately 22% of the study region investigated here (Fig. 1a), forested grid cells contained just over 34% of the total 13 March SWE volume, a volume about 10% higher than the snow volume contained in the next-largest landcover type (Fig. 6a). In forested grid cells, SWE simulated by the open loop simulation were biased high by approximately 87 mm (+150%) on average (Fig. 6), with a mean absolute error of 111 mm (Table 2). These errors were propagated into the simulation with data assimilation without the forest strategy. Fortunately, the ratio between modeled SWE and synthetic SWE observations in forested grid cells and the nearest canopy-free grid cells had high levels of similarity. Therefore, estimating snow in forest regions using the nearest canopy-free pixels (Fig. 2) improved snow simulations significantly (Fig. 3d, Fig. 4d, and Fig. 5c and 5f). In fact, snow simulated in forest landscapes using data assimilation with the forest strategy agreed well with the nature run, exhibiting a 13 March SWE average bias in forested grid cells of only 14 mm (+8%) (Fig. 6), and a mean absolute error of 27 mm. This forest strategy resulted in large-scale improvements to total domain SWE (Fig. 5), reducing the 13 March full-domain SWE volume bias by 28%, and improving the spatial coefficient of correlation by 0.12, relative to the data assimilation simulation without the forest strategy.

https://doi.org/10.5194/egusphere-2023-1603
Preprint. Discussion started: 18 July 2023

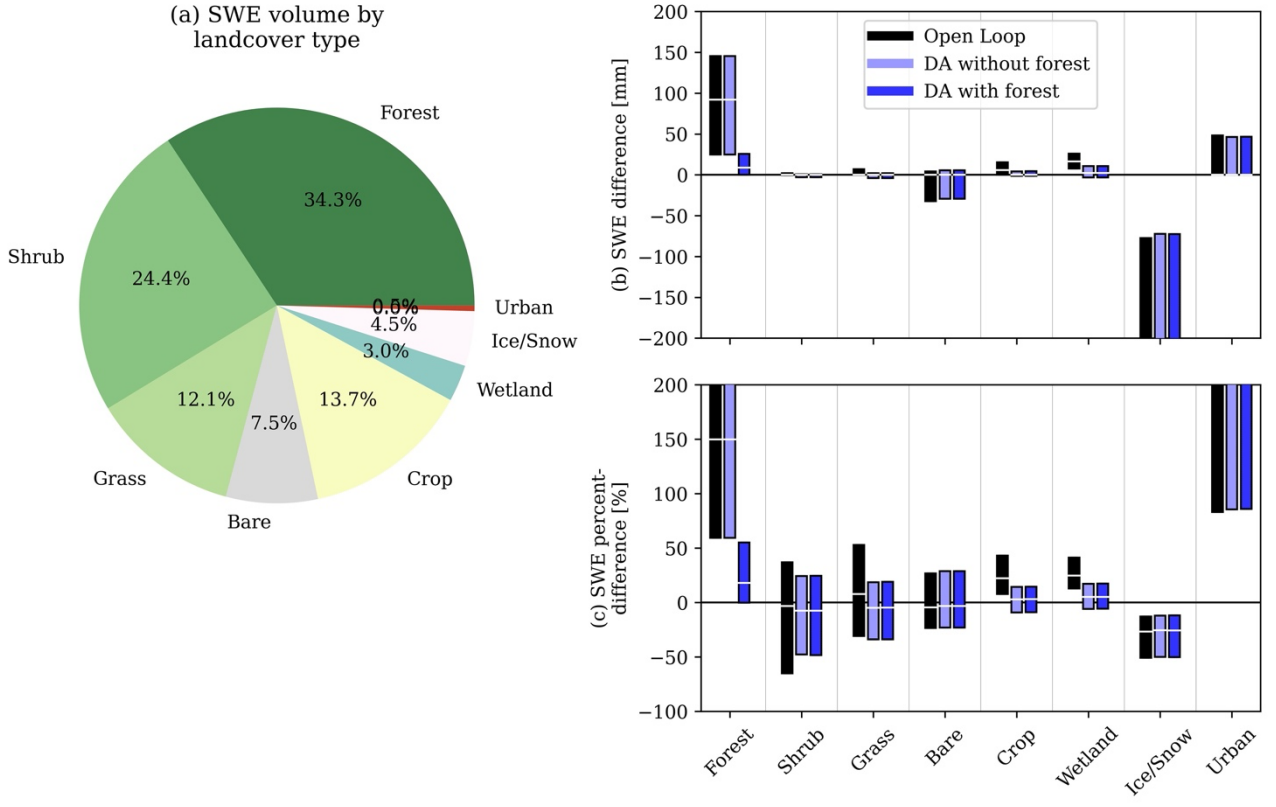

Figure 6. SWE volume on 13 March 2019 broken down by landcover type in subplot a. For each landcover type, the interquartile range and median of SWE differences (b) and SWE percent-differences (c) are calculated for the open loop simulation (black) and each simulation with data assimilation (blue bars). SWE differences (b) and (c) are calculated relative to the nature run.

The comparisons above focused on mean DJF SWE and SWE from the date nearest peak snow volume (13 March, 2019). However, assimilating the synthetic SWE data also improved estimates of snow water resources throughout the duration of the water year, even in periods when most snow-covered regions were experiencing snowmelt and synthetic observations were masked. For example, in the Upper Colorado basin, approximately 75% of the basin had DJF snow cover with little or no winter snowmelt (Fig. 7). The simulation with data assimilation and the forest strategy substantially improved basin-mean SWE evolution in the snow accumulation season in this basin (Fig. 7, October - March). However, snowmelt onset in the March, April, and May (MAM) months increased the number of grid cells experiencing snowmelt from the open loop model outputs, reducing the number of grid cells that could be observed by the synthetic SAR observations to approximately 5%, on average, over this period of time. Despite this, since the simulation with data assimilation improved the volume, timing, and spatial distribution of peak SWE, mean SWE evolution tracked the nature run simulation significantly better than the open loop simulation in the spring snowmelt period. In fact, relative to the nature run, MAM SWE from the open loop simulations was biased high by approximately 63%, on average, in the Upper Colorado (Table 2). The simulation with data

https://doi.org/10.5194/egusphere-2023-1603
Preprint. Discussion started: 18 July 2023

assimilation using the forest strategy improved this bias to less than 1%, on average, over the same period. In this study, simulations using Noah-MP (open loop and data assimilation simulations) melted snow more rapidly in the later-half of the spring snowmelt season than the nature run simulation which evolved SWE using SnowModel (Section 2.1). Therefore, although peak SWE volume, peak SWE timing, and MAM SWE were improved by data assimilation, the timing of snow disappearance for the simulation with data assimilation using the forest strategy was approximately 18 days earlier than the nature run in the Upper Colorado.

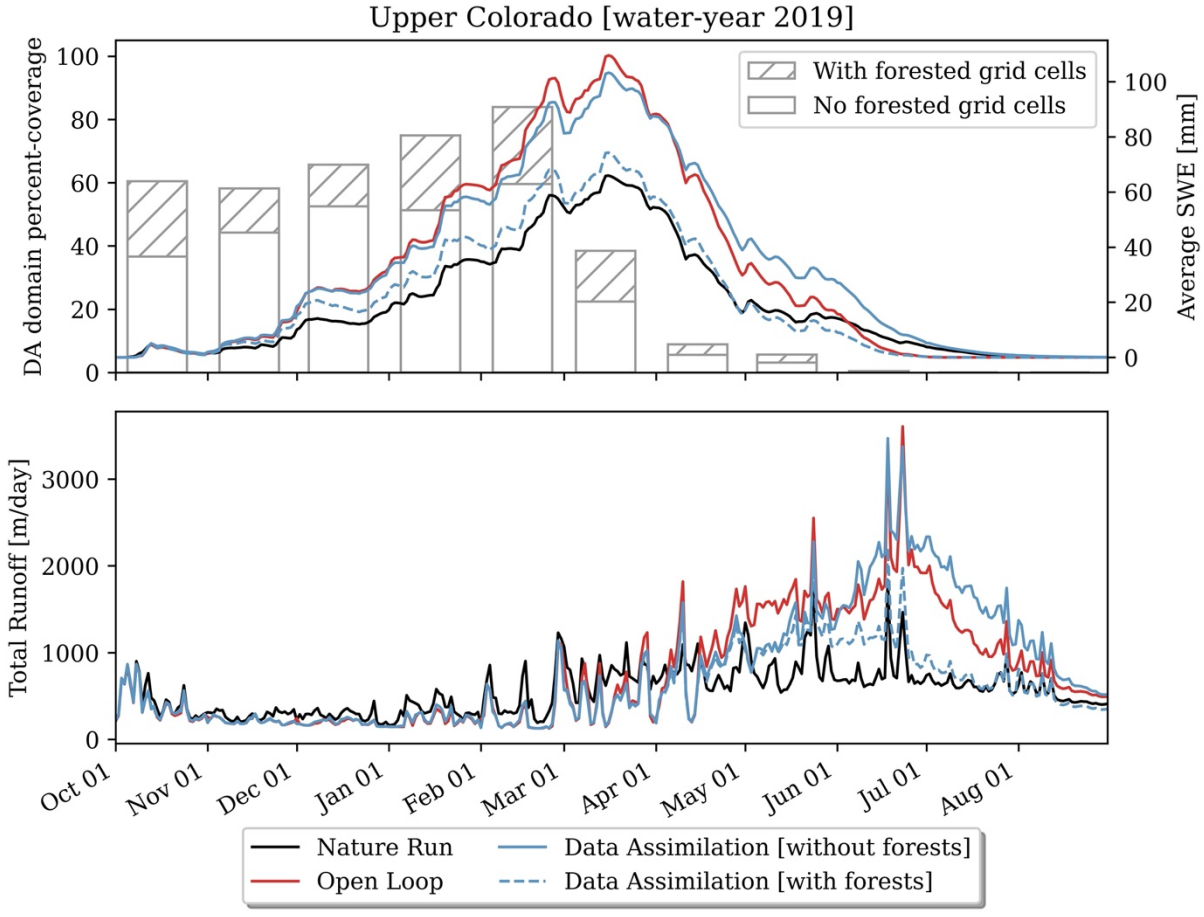

Figure 7. Time series comparison of basin-mean SWE (top) and total runoff (bottom) between the open loop, nature run, and simulations assimilating the synthetic observations, both with and without the forest strategy in the Upper Colorado basin. Dashed bars in the top plot represent the monthly percentage of the Upper Colorado grid cells with no snowmelt. Solid bars also exclude grid cells with forest coverage.

Much like the Upper Colorado Basin, SWE simulated by the open loop simulation in the Pacific Northwest (Fig. S5) was biased high for the entirety of the snow season. Both domains also had greater than 80% synthetic snow observation coverage in March (including grid cells that filled snow estimates using the forest strategy), and as a result, the simulation

https://doi.org/10.5194/egusphere-2023-1603
Preprint. Discussion started: 18 July 2023

with data assimilation using the forest strategy closely matched SWE from the nature run. However, both of these domains had a significant portion of the seasonal snowpack in forested landcover (Fig. 7 and Fig. S5, difference between the hatched and solid bars). These grid cells had winter SWE estimates from the open loop simulation that were predominately high-biased (Fig. 3 and Fig. 5). Therefore, although data assimilation improved winter SWE in non-forested landcover types (Fig. 6), the simulation without the forest strategy caused little-to-no improvement in the simulated domain mean peak SWE (Table 2). This highlights the value of the forest strategy used here (Fig. 2), which drew information from synthetic observations in relatively few nearby pixels to infer the mean snow volume in forested grid cells. Given the four basins investigated in this study, a far smaller volume of snow existed in forested landcover for the California (Fig. S6) and Great Basins (Fig. S4), resulting in DJF domain-mean SWE evolution that was more similar between the simulations with and without the forest strategy. We expect results in these domains to be more indicative of the value of winter SAR observations in less-vegetated snowy landscapes, such as Tundra and Prairie snow regimes (Sturm and Liston, 2021).

Finally, the improvements to the spatial and temporal estimates of SWE discussed above had trickle-down improvements on simulated runoff. For example, in the Upper Colorado (Fig. 7), total annual runoff from the open loop simulation was biased high by approximately 35%, relative to the nature run. This error was driven most by high-biased winter snow accumulation, which nearly doubled the melt season (March – July) runoff estimated by the nature run simulation. Here, by assimilating the synthetic SWE observations, and estimating forest snowpack from the relationship between modeled and observed SWE from the nearest canopy-free pixels, total annual streamflow in this domain was improved to within 1%. Not only was domain total runoff improved, but the seasonal evolution of high and low-flows vital for water management and planning was also improved. This improved the Nash-Sutcliffe Efficiency (NSE) from –2.59 to 0.22 between the open loop simulation and simulation with data assimilation employing the forest strategy (Table 2). These results were similar for the Pacific Northwest, which had an NSE that improved from –0.17 to 0.39. Here, due to the smaller changes to SWE and more-rapid snowmelt simulated by Noah-MP, changes to runoff from data assimilation in California and the Great Basin were small (Table 2).

4. Discussion

The differences between the open loop simulation and nature run in this study were representative of typical snow modeling errors reported in the literature (e.g., Franz et al., 2010; Garousi-Nejad and Tarboton, 2022; Kim et al, 2021). The greatest source of these snow modeling errors is commonly errors in meteorological forcing data, and in particular, biases in precipitation (Garousi-Nejad and Tarboton, 2022; Henn et al., 2018; Pflug et al., 2021; Raleigh and Lundquist, 2012; Wayand et al., 2013). These biases are especially prevalent in the portions of the earth's surface with the greatest volumes of snow, such as the tundra and montane regions (Kim et al., 2021), where ground observations and observation station maintenance are hindered by harsh winter conditions and inaccessibility. This suggests that the greatest need for improving global estimates of snow is improved estimates of snow accumulation in remote, under sampled landscapes. Here, we expect that the SAR

https://doi.org/10.5194/egusphere-2023-1603
Preprint. Discussion started: 18 July 2023

observations evaluated in this study could address these needs. For example, assimilating SAR observations at 10 – 14 day intervals with the observational error characteristics reported in Sect. 2.2, improved midlatitude winter SWE volume by approximately 22%, on average (Table 2). In unforested landscapes, which account for a majority of the Earth's snow water storage (Kim et al., 2021), assimilation improved the mean SWE bias at peak-SWE timing to within 1%, on average, and reduced the standard deviation of errors by approximately 45 mm (~85%) (Fig. 6).

Despite the benefits discussed above, SAR observations have known limitations in forested landscapes where the canopy overstory obstructs retrievals from the underlying snowpack (Huang et al., 2019; Ruiz et al., 2022; Tsang et al., 2022). Therefore, this study was designed to investigate a forest strategy that uses the relationship between modeled SWE estimates and synthetic SWE observations from neighboring grid cells as the basis for inferring snow distribution in regions with forested landcover (Fig. 2). To focus on the benefits of this approach, we chose a domain (Fig. 1) that included both significant forest spatial coverage (22%) with disproportionate amounts of winter snow (34%) within the forested pixels (Fig. 6). Relative to the open loop simulation, the simulation with data assimilation and the forest strategy dramatically improved the spatial distribution of SWE (e.g., Fig. 3 and Fig. 4) and the resulting SWE biases at peak-snowpack timing (Fig. 5). In fact, in forested grid cells, SWE on 13 March was only biased by 14 mm (mean absolute error of 27 mm), on average, for the simulation with data assimilation and the forest strategy. This was opposed to the open loop simulation, which was biased by 87 mm (mean absolute error of 111 mm) over the same regions and date. Despite the fact that the two simulations with data assimilation agreed in all grid cells except forested grid cells, the simulation employing the forest strategy had a mean absolute error (17 mm) across the full modeling region that was approximately 51% smaller than the simulation without the forest strategy.

This research shows how a modeling framework and relatively few observations can be used to gap-fill estimates of snow in regions where remote sensing observations from a future platform may be most challenged. Despite the fact that snowpack with properties able to be retrieved by SAR instrumentation (i.e., canopy-free landcover and no snowmelt) sometimes only accounted for only small portions of a modeling domain (e.g., Fig. 7), SWE from the model and SAR observations in nearby canopy-free grid cells were predictive of the snow in forested grid cells. We hypothesize that this could have partly been driven by the 250 m resolution of synthetic observations and simulations. At this length scale, snow distribution is typically driven by processes like synoptic weather patterns and their interaction (e.g., orographic lapse rates, wind loading/sheltering, terrain-shading, etc.) with static topographical features like elevation, slope, and aspect (e.g., Clark et al., 2011; Lehning et al., 2011; McGrath et al., 2018; Minder et al., 2008; Trujillo et al., 2007). However, we acknowledge that snow in forested and open grid cells is subject to different snow processes. In fact, the nature run simulation used here attempts to simulate snow-canopy interactions, such as snow interception and solar shading from the canopy overstory (Liston and Elder, 2006). Here, since we focus predominantly on model improvements from data assimilation in the SWE accumulation season, we hypothesize that the primary difference between SWE accumulation in forested pixels, and the nearest canopy-free grid cells could be driven by canopy interception, or the lack thereof. In other words, inferring forested snowpack using the nearest canopy-free grid

https://doi.org/10.5194/egusphere-2023-1603
Preprint. Discussion started: 18 July 2023

cells could bias snow in forested regions where snow processes differ slightly. While the forest strategy improved SWE simulated in forested grid cells at the date of peak-SWE volume, SWE was still biased high relative to the nature run (Fig. 6). We hypothesize that a correction factor, based on variables like forest canopy type, vegetation density, and temperature during snowfall, all of which influence snow interception, could be used to facilitate the difference in snow accumulation expected between a forest pixel and SWE observations from nearby canopy-free grid cells. This approach will be a topic of future research. However, since errors with precipitation are often the overwhelming source of model errors, we hypothesize that the forest strategy (Fig. 2), which corrected modeled SWE in forested areas using the ratio between modeled and observed SWE in nearby open areas, was well-suited to correct precipitation biases.

This study tested a simple model setup using a popular land surface model (Noah-MP) and Kalman-based data assimilation procedure. This data assimilation procedure updated modeled snow states, like snow depth and SWE, based only on synthetic SWE observations at 10 – 14 day temporal frequencies where/when snowmelt was not occurring. We expect that the results presented here could represent the lower-bound of performance that could be achieved from a real-time modeling framework that could accompany a space-borne SAR remote sensing platform. For example, many studies have demonstrated repeatable patterns of snow accumulation in years with similar winter meteorological characteristics (e.g., Deems et al., 2008; Pflug et al, 2022; Schirmer et al., 2011; Sturm and Wagner, 2010; Woodruff and Qualls, 2019). This suggests that retrospective information about snow distribution patterns in previous years, could be used as the basis for extrapolating and updating snow model states in grid cells not covered by SAR observations on a given date. From the modeling perspective, only 5 ensemble members were used in the Ensemble-Kalman data assimilation (Sec 2.3), when a larger ensemble of simulations may have improved uncertainty characterization simulated snow and hydrological states even more. This study also assumed that synthetic SAR observations were unable to observe snow in all forested landscapes, when retrievals of snow in forested stands could be achievable for some forested regions with smaller tree cover fractions and biomass (Montomoli et al., 2015; Tsang et al., 2022). Finally, the SAR configuration tested here had 10 – 14 day repeat times, but future satellite configurations with more-frequent observational repeats could be possible. Despite all of these conservative assumptions, the difference between the open loop simulation (representative of current modeling accuracies), and the simulation with synthetic observation data assimilation using the forest strategy, demonstrated large-magnitude and widespread improvements to real-time estimates of winter SWE and the associated improvement to spring SWE and runoff. Therefore, we expect the findings of this study, particularly the strategy to extend the observational utility to forested areas, to significantly aid in the full exploitation of the information from a future SAR-based snow satellite mission.

5. **Conclusion**

Global estimates of snow volume and distribution have uncertainties stemming from limited snow observations and biases in meteorological forcing data. These uncertainties stress the need for a global snow-focused satellite remote sensing platform. Here, we investigate the degree to which synthetic observations of snow water equivalent (SWE)

https://doi.org/10.5194/egusphere-2023-1603
Preprint. Discussion started: 18 July 2023

representative of a Synthetic Aperture Radar (SAR) remote sensing platform, could correct common snow modeling errors and provide spatiotemporally continuous SWE estimates. We investigate this using an Observation System Simulation Experiment, specifically investigating how much snow simulated using a popular land surface model and meteorological forcing dataset, could be improved by assimilating synthetic SAR observations of SWE.

The difference between the open loop simulation and the nature run were representative of common modeling errors. Snow simulated by the open loop simulation had larger winter snow extents, and total snow volume that was biased high by approximately 35%. The open loop simulation also simulated snow that was more spatially homogeneous, underestimating the variability across variations in topography and underestimating lower-elevation snowmelt from the nature run. Assimilating the synthetic SWE observations improved SWE simulated in the shrub, grass, crop, bare-ground, and wetland land cover types. In fact, SWE biases on the date of domain peak SWE volume (13 March 2019) in these landcover types improved from 14% for the open loop simulation to within 1% after data assimilation. However, despite only covering 22% of the study area, forested grid cells contained just over 34% of the domain SWE on 13 March. The open loop simulation and the simulation with data assimilation without the forest strategy had SWE that was high biased by 150% (87 mm), on average, in these forested grid cells. The relationship between modeled SWE and synthetic SWE observations in forested grid cells exhibited similarities with the nearest canopy-free grid cells. Therefore, SWE in forested regions was able to be inferred using the simple modeling framework and synthetic SAR observations from nearby canopy-free grid cells. In fact, the simulation with data assimilation using this forest gap-filling strategy substantially improved SWE biases to 4% (~22% improvement) at peak-SWE timing, with a SWE mean absolute error of 17 mm (24 mm improvement) and spatial correlation of 0.91 (0.17 improvement) across the Western US

Improvements in winter SWE accumulation also improved estimates of melt-season SWE evolution and total runoff in four major Western United States hydrological basins, even in periods when winter snowmelt greatly reduced the number of grid cells that could be observed by the synthetic SWE observations. In fact, in the Upper Colorado River basin, melt season SWE biases improved from 63% to less than 1% after assimilation, and the runoff Nash Sutcliffe Efficiency improved from -2.59 to 0.22. These results demonstrate the value of SAR observations and simple spatial-filling strategies in grid cells where SAR retrievals could be obstructed by the canopy. Here, we expect our results to represent a lower-boundary of model performance which could be improved further by more robust assimilation approaches, more-frequent SAR observations, and adaptations to the forest gap-filling strategy developed here. However, our results also show that widespread improvements to global SWE could be available in near real-time provided data assimilation approaches and a SAR remote sensing platform.

https://doi.org/10.5194/egusphere-2023-1603
Preprint. Discussion started: 18 July 2023

Code availability: The Land Information System (LIS; lis.gsfc.nasa.gov) framework used to perform the nature run, open loop, and data assimilation simulations from this study can be accessed from a GitHub public repository (https://github.com/NASA-LIS/LISF). Model documentation and LIS tutorials can also be accessed from this repository. Users are encouraged to reference Kumar et al. (2006) for more information on LIS. The Trade-space Analysis Tool for designing Constellations (TAT-C) tool is currently available on-request for federal employees and contractors (https://software.nasa.gov/software/GSC-18399-1).

Data availability: The model outputs and data necessary to reproduce the figures and statistics reported in this study can be found at https://www.hydroshare.org/resource/e0ad80f818bf4062a335e9e0d7362834/. This repository includes domain static variables, such as land cover, elevation, and spatial coordinates, in addition to model outputs of winter-average SWE, SWE at the date of peak-SWE volume (13 March 2019), and basin-aggregated SWE and runoff. MERRA-2 forcing data can be accessed from the Goddard Earth Sciences Data and Information Services Center (GES DISC, https://disc.gsfc.nasa.gov/).

Author contributions: CV and SK coordinated the manuscript question and research methodology. SK adapted LIS model source code to implement the forest gap-filling strategy in Sect. 2.4. MW set up the model domains and model configurations, and performed the open loop simulation. EC assisted with generating the synthetic SWE observations. With assistance from KA, JP performed code developments for the simulations using both the Noah-MP and coupled SnowModel models. KA implemented the SnowModel code and parameters into LIS and LDT. JP also performed the nature run and both data assimilation simulations. The manuscript was written provided text, figures, and feedback from all coauthors.

Competing interests: The authors declare that they have no conflict of interest.

Acknowledgements: This work was supported by the funding from the NASA Terrestrial Hydrology program. Computing was supported by the NASA Center for Climate Simulation (NCCS).

References

Arsenault, K.R., Kumar, S.V., Geiger, J.V., Wang, S., Kemp, E., Mocko, D.M., Beaudoing, H.K., Getirana, A., Navari, M., Li, B., Jacob, J., Wegiel, J., Peters-Lidard, C.D.: The Land surface Data Toolkit (LDT v7.2) – a data fusion environment for land data assimilation systems. Geoscientific Model Development 11, 3605–3621. https://doi.org/10.5194/gmd-11-3605-2018, 2018.

Barnett, T.P., Adam, J.C., Lettenmaier, D.P.:Potential impacts of a warming climate on water availability in snow-dominated regions. Nature 438, 303. https://doi.org/10.1038/nature04141, 2005.

Barry, R.G.: The Role of Snow and Ice in the Global Climate System: A Review. Polar Geography 26, 235–246. https://doi.org/10.1080/789610195, 2002.

Best, M.J., Pryor, M., Clark, D.B., Rooney, G.G., Essery, R.L.H., Ménard, C.B., Edwards, J.M., Hendry, M.A., Porson, A., Gedney, N., Mercado, L.M., Sitch, S., Blyth, E., Boucher, O., Cox, P.M., Grimmond, C.S.B., Harding, R.J.: The Joint

https://doi.org/10.5194/egusphere-2023-1603
Preprint. Discussion started: 18 July 2023

UK Land Environment Simulator (JULES), model description – Part 1: Energy and water fluxes. Geoscientific Model Development 4, 677–699. https://doi.org/10.5194/gmd-4-677-2011, 2011.

Cho, E., Vuyovich, C.M., Kumar, S.V., Wrzesien, M.L., Kim, R.S.: Evaluating the Utility of Active Microwave Observations as a Snow Mission Concept Using Observing System Simulation Experiments. The Cryosphere Discussions 1–24. https://doi.org/10.5194/tc-2022-220, 2022.

Clark, M.P., Hendrikx, J., Slater, A.G., Kavetski, D., Anderson, B., Cullen, N.J., Kerr, T., Hreinsson, E.Ö., Woods, R.A.: Representing spatial variability of snow water equivalent in hydrologic and land-surface models: A review. Water Resources Research 47. https://doi.org/10.1029/2011WR010745, 2011.

De Lannoy, G.J.M., Reichle, R.H., Arsenault, K.R., Houser, P.R., Kumar, S., Verhoest, N.E.C., Pauwels, V.R.N.: Multiscale assimilation of Advanced Microwave Scanning Radiometer–EOS snow water equivalent and Moderate Resolution Imaging Spectroradiometer snow cover fraction observations in northern Colorado. Water Resources Research 48. https://doi.org/10.1029/2011WR010588, 2012.

Deems, J.S., Fassnacht, S.R., Elder, K.J.: Interannual Consistency in Fractal Snow Depth Patterns at Two Colorado Mountain Sites. J. Hydrometeor 9, 977–988. https://doi.org/10.1175/2008JHM901.1, 2008.

Ek, M.B., Mitchell, K.E., Lin, Y., Rogers, E., Grunmann, P., Koren, V., Gayno, G., Tarpley, J.D.: Implementation of Noah land surface model advances in the National Centers for Environmental Prediction operational mesoscale Eta model. Journal of Geophysical Research: Atmospheres 108. https://doi.org/10.1029/2002JD003296, 2003.

Errico, R.M., Yang, R., Masutani, M., Woollen, J.S.: The estimation of analysis error characteristics using an observation systems simulation experiment. Meteorologische Zeitschrift 16, 695–708, 2007.

Franz, K.J., Butcher, P., Ajami, N.K.: Addressing snow model uncertainty for hydrologic prediction. Advances in Water Resources 33, 820–832. https://doi.org/10.1016/j.advwatres.2010.05.004, 2010.

Garnaud, C., Bélair, S., Carrera, M.L., Derksen, C., Bilodeau, B., Abrahamowicz, M., Gauthier, N., Vionnet, V.: Quantifying Snow Mass Mission Concept Trade-Offs Using an Observing System Simulation Experiment. Journal of Hydrometeorology 20, 155–173. https://doi.org/10.1175/JHM-D-17-0241.1, 2019.

Garousi-Nejad, I., Tarboton, D.G.: A comparison of National Water Model retrospective analysis snow outputs at snow telemetry sites across the Western United States. Hydrological Processes 36, e14469. https://doi.org/10.1002/hyp.14469, 2022.

Gelaro, R., McCarty, W., Suárez, M.J., Todling, R., Molod, A., Takacs, L., Randles, C.A., Darmenov, A., Bosilovich, M.G., Reichle, R., Wargan, K., Coy, L., Cullather, R., Draper, C., Akella, S., Buchard, V., Conaty, A., Silva, A.M. da, Gu, W., Kim, G.-K., Koster, R., Lucchesi, R., Merkova, D., Nielsen, J.E., Partyka, G., Pawson, S., Putman, W., Rienecker, M., Schubert, S.D., Sienkiewicz, M., Zhao, B.: The Modern-Era Retrospective Analysis for Research and Applications, Version 2 (MERRA-2). Journal of Climate 30, 5419–5454. https://doi.org/10.1175/JCLI-D-16-0758.1, 2017.

Henn, B., Newman, A.J., Livneh, B., Daly, C., Lundquist, J.D.: An assessment of differences in gridded precipitation datasets in complex terrain. Journal of Hydrology 556, 1205–1219. https://doi.org/10.1016/j.jhydrol.2017.03.008, 2018.

Hiemstra, C.A., Liston, G.E., Reiners, W.A.: Snow Redistribution by Wind and Interactions with Vegetation at Upper Treeline in the Medicine Bow Mountains, Wyoming, U.S.A. Arctic, Antarctic, and Alpine Research 34, 262–273. https://doi.org/10.1080/15230430.2002.12003493, 2002.

Huang, H., Tsang, L., Colliander, A., Yueh, S.H.: Propagation of Waves in Randomly Distributed Cylinders Using Three-Dimensional Vector Cylindrical Wave Expansions in Foldy–Lax Equations. IEEE Journal on Multiscale and Multiphysics Computational Techniques 4, 214–226. https://doi.org/10.1109/JMMCT.2019.2948022, 2019.

Kim, R.S., Kumar, S., Vuyovich, C., Houser, P., Lundquist, J., Mudryk, L., Durand, M., Barros, A., Kim, E.J., Forman, B.A., Gutmann, E.D., Wrzesien, M.L., Garnaud, C., Sandells, M., Marshall, H.-P., Cristea, N., Pflug, J.M., Johnston, J., Cao, Y., Mocko, D., Wang, S.: Snow Ensemble Uncertainty Project (SEUP): quantification of snow water equivalent uncertainty across North America via ensemble land surface modeling. The Cryosphere 15, 771–791. https://doi.org/10.5194/tc-15-771-2021, 2021.

Koster, R.D., Mahanama, S.P.P., Livneh, B., Lettenmaier, D.P., Reichle, R.H.: Skill in streamflow forecasts derived from large-scale estimates of soil moisture and snow. Nature Geosci 3, 613–616. https://doi.org/10.1038/ngeo944, 2010.

https://doi.org/10.5194/egusphere-2023-1603
Preprint. Discussion started: 18 July 2023

Koster, R.D., Suarez, M.J., Ducharne, A., Stieglitz, M., Kumar, P.: A catchment-based approach to modeling land surface processes in a general circulation model: 1. Model structure. Journal of Geophysical Research: Atmospheres 105, 24809–24822. https://doi.org/10.1029/2000JD900327, 2000.

Kumar, S.V., Kolassa, J., Reichle, R., Crow, W., de Lannoy, G., de Rosnay, P., MacBean, N., Girotto, M., Fox, A., Quaife, T., Draper, C., Forman, B., Balsamo, G., Steele-Dunne, S., Albergel, C., Bonan, B., Calvet, J.-C., Dong, J., Liddy, H., Ruston, B.: An Agenda for Land Data Assimilation Priorities: Realizing the Promise of Terrestrial Water, Energy, and Vegetation Observations From Space. Journal of Advances in Modeling Earth Systems 14, e2022MS003259. https://doi.org/10.1029/2022MS003259, 2022.

Kumar, S.V., Peters-Lidard, C.D., Tian, Y., Houser, P.R., Geiger, J., Olden, S., Lighty, L., Eastman, J.L., Doty, B., Dirmeyer, P., Adams, J., Mitchell, K., Wood, E.F., Sheffield, J.: Land information system: An interoperable framework for high resolution land surface modeling. Environmental Modelling & Software 21, 1402–1415. https://doi.org/10.1016/j.envsoft.2005.07.004, 2006.

Kwon, Y., Yoon, Y., Forman, B.A., Kumar, S.V., Wang, L.: Quantifying the observational requirements of a space-borne LiDAR snow mission. Journal of Hydrology 601, 126709. https://doi.org/10.1016/j.jhydrol.2021.126709, 2021.

Lahmers, T.M., Kumar, S.V., Rosen, D., Dugger, A., Gochis, D.J., Santanello, J.A., Gangodagamage, C., Dunlap, R.: Assimilation of NASA's Airborne Snow Observatory Snow Measurements for Improved Hydrological Modeling: A Case Study Enabled by the Coupled LIS/WRF-Hydro System. Water Resources Research 58, e2021WR029867. https://doi.org/10.1029/2021WR029867, 2022.

Le Moigne, J., Dabney, P., de Weck, O., Foreman, V., Grogan, P., Holland, M., Hughes, S., Nag, S.: Tradespace analysis tool for designing constellations (TAT-C), in: 2017 IEEE International Geoscience and Remote Sensing Symposium (IGARSS). IEEE, pp. 1181–1184, 2017.

Lehning, M., Grünewald, T., Schirmer, M.: Mountain snow distribution governed by an altitudinal gradient and terrain roughness. Geophysical Research Letters 38. https://doi.org/10.1029/2011GL048927, 2011.

Li, D., Wrzesien, M.L., Durand, M., Adam, J., Lettenmaier, D.P.: How much runoff originates as snow in the western United States, and how will that change in the future? Geophysical Research Letters 44, 6163–6172. https://doi.org/10.1002/2017GL073551, 2017.

Liang, X., Lettenmaier, D.P., Wood, E.F., Burges, S.J.: A simple hydrologically based model of land surface water and energy fluxes for general circulation models. Journal of Geophysical Research: Atmospheres 99, 14415–14428. https://doi.org/10.1029/94JD00483, 1994.

Lievens, H., Demuzere, M., Marshall, H.P., Reichle, R.H., Brucker, L., de Rosnay, P., Dumont, M., Girotto, M., Immerzeel, W.W., Jonas, T., Kim, E.J., Koch, I., Marty, C., Saloranta, T., Schober, J., De Lannoy, G.J.M.: Snow depth variability in the Northern Hemisphere mountains observed from space. Nature Communications, 2019.

Liston, G.E., Elder, K.: A Distributed Snow-Evolution Modeling System (SnowModel). Journal of Hydrometeorology 7, 1259–1276. https://doi.org/10.1175/JHM548.1, 2006.

Liston, G.E., Perham, C.J., Shideler, R.T., Cheuvront, A.N.: Modeling snowdrift habitat for polar bear dens. Ecological Modelling 320, 114–134. https://doi.org/10.1016/j.ecolmodel.2015.09.010, 2016.

Livneh, B., Badger, A.M.: Drought less predictable under declining future snowpack. Nat. Clim. Chang. 10, 452–458. https://doi.org/10.1038/s41558-020-0754-8, 2020.

Mahoney, P.J., Liston, G.E., LaPoint, S., Gurarie, E., Mangipane, B., Wells, A.G., Brinkman, T.J., Eitel, J.U.H., Hebblewhite, M., Nolin, A.W., Boelman, N., Prugh, L.R.: Navigating snowscapes: scale-dependent responses of mountain sheep to snowpack properties. Ecological Applications 28, 1715–1729. https://doi.org/10.1002/eap.1773, 2018.

McGrath, D., Sass, L., O'Neel, S., McNeil, C., Candela, S.G., Baker, E.H., Marshall, H.P.: Interannual snow accumulation variability on glaciers derived from repeat, spatially extensive ground-penetrating radar surveys. The Cryosphere 12, 3617–3633. https://doi.org/10.5194/tc-12-3617-2018, 2018.

Mernild, S.H., Liston, G.E., Hiemstra, C., Wilson, R.: The Andes Cordillera. Part III: glacier surface mass balance and contribution to sea level rise (1979–2014). International Journal of Climatology 37, 3154–3174. https://doi.org/10.1002/joc.4907, 2017.

Minder, J.R., Durran, D.R., Roe, G.H., Anders, A.M.: The climatology of small-scale orographic precipitation over the Olympic Mountains: Patterns and processes. Quarterly Journal of the Royal Meteorological Society 134, 817–839. https://doi.org/10.1002/qj.258, 2008.

https://doi.org/10.5194/egusphere-2023-1603
Preprint. Discussion started: 18 July 2023

Montomoli, F., Macelloni, G., Brogioni, M., Lemmetyinen, J., Cohen, J., Rott, H.: Observations and simulation of multifrequency SAR data over a snow-covered boreal forest. IEEE journal of selected topics in applied earth observations and remote sensing 9, 1216–1228, 2015.

Niu, G., Yang, Z., Mitchell, K.E., Chen, F., Ek, M.B., Barlage, M., Kumar, A., Manning, K., Niyogi, D., Rosero, E., Tewari, M., Xia, Y.: The community Noah land surface model with multiparameterization options (Noah-MP): 1. Model description and evaluation with local-scale measurements. Journal of Geophysical Research: Atmospheres 116. https://doi.org/10.1029/2010JD015139, 2011.

Niu, G.-Y., Yang, Z.-L.: Effects of vegetation canopy processes on snow surface energy and mass balances. Journal of Geophysical Research: Atmospheres 109. https://doi.org/10.1029/2004JD004884, 2004.

Painter, T.H., Berisford, D.F., Boardman, J.W., Bormann, K.J., Deems, J.S., Gehrke, F., Hedrick, A., Joyce, M., Laidlaw, R., Marks, D., Mattmann, C., McGurk, B., Ramirez, P., Richardson, M., Skiles, S.M., Seidel, F.C., Winstral, A.: The Airborne Snow Observatory: Fusion of scanning lidar, imaging spectrometer, and physically-based modeling for mapping snow water equivalent and snow albedo. Remote Sensing of Environment 184, 139–152. https://doi.org/10.1016/j.rse.2016.06.018, 2016.

Pflug, J.M., Hughes, M., Lundquist, J.D.: Downscaling snow deposition using historic snow depth patterns: Diagnosing limitations from snowfall biases, winter snow losses, and interannual snow pattern repeatability. Water Resources Research e2021WR029999. https://doi.org/10.1029/2021WR029999, 2021.

Pflug, J.M., Margulis, S.A., Lundquist, J.D.: Inferring watershed-scale mean snowfall magnitude and distribution using multidecadal snow reanalysis patterns and snow pillow observations. Hydrological Processes 36, e14581, 2022.

Raleigh, M.S., Lundquist, J.D.: Comparing and combining SWE estimates from the SNOW-17 model using PRISM and SWE reconstruction. Water Resources Research 48. https://doi.org/10.1029/2011WR010542, 2012.

Reichle, R.H., McLaughlin, D.B., Entekhabi, D.: Hydrologic Data Assimilation with the Ensemble Kalman Filter. Monthly Weather Review 130, 103–114. https://doi.org/10.1175/1520-0493(2002)130<0103:HDAWTE>2.0.CO;2, 2002.

Ruiz, J.J., Lemmetyinen, J., Kontu, A., Tarvainen, R., Vehmas, R., Pulliainen, J., Praks, J.: Investigation of Environmental Effects on Coherence Loss in SAR Interferometry for Snow Water Equivalent Retrieval. IEEE Transactions on Geoscience and Remote Sensing 60, 1–15. https://doi.org/10.1109/TGRS.2022.3223760, 2022.

Schirmer, M., Wirz, V., Clifton, A., Lehning, M.: Persistence in intra-annual snow depth distribution: 1. Measurements and topographic control: PERSISTENT SNOW DEPTH DEVELOPMENT, 1. Water Resources Research 47. https://doi.org/10.1029/2010WR009426, 2011.

Sturm, M., Wagner, A.M.: Using repeated patterns in snow distribution modeling: An Arctic example. Water Resources Research 46, 2010.

Terzago, S., Bongiovanni, G., von Hardenberg, J.: Seasonal forecasting of snow resources at Alpine sites. Hydrology and Earth System Sciences 27, 519–542. https://doi.org/10.5194/hess-27-519-2023, 2023.

Trujillo, E., Ramírez, J.A., Elder, K.J.: Topographic, meteorologic, and canopy controls on the scaling characteristics of the spatial distribution of snow depth fields. Water Resources Research 43, 2007.

Tsang, L., Durand, M., Derksen, C., Barros, A.P., Kang, D.-H., Lievens, H., Marshall, H.-P., Zhu, J., Johnson, J., King, J., Lemmetyinen, J., Sandells, M., Rutter, N., Siqueira, P., Nolin, A., Osmanoglu, B., Vuyovich, C., Kim, E., Taylor, D., Merkouriadi, I., Brucker, L., Navari, M., Dumont, M., Kelly, R., Kim, R.S., Liao, T.-H., Borah, F., Xu, X.: Review article: Global monitoring of snow water equivalent using high-frequency radar remote sensing. The Cryosphere 16, 3531–3573. https://doi.org/10.5194/tc-16-3531-2022, 2022.

Wayand, N.E., Hamlet, A.F., Hughes, M., Feld, S.I., Lundquist, J.D.: Intercomparison of Meteorological Forcing Data from Empirical and Mesoscale Model Sources in the North Fork American River Basin in Northern Sierra Nevada, California. Journal of Hydrometeorology 14, 677–699. https://doi.org/10.1175/JHM-D-12-0102.1, 2013.

Woodruff, C.D., Qualls, R.J.: Recurrent Snowmelt Pattern Synthesis using Principal Component Analysis of Multi-Year Remotely Sensed Snow Cover. Water Resources Research 55, 6869–6885. https://doi.org/10.1029/2018WR024546, 2019.

Wrzesien, M., Kumar, S.V., Vuyovich, C., Kim, R.S., Cho, E., Pflug, J.M., Konapala, G., Arsenault, K.R.: Merging remote sensing and models to improve performance and accessibility of snow information, AGU Fall Meeting, Conference on Hydrology, 2022.

https://doi.org/10.5194/egusphere-2023-1603
Preprint. Discussion started: 18 July 2023

Wrzesien, M.L., Kumar, S., Vuyovich, C., Gutmann, E.D., Kim, R.S., Forman, B.A., Durand, M., Raleigh, M.S., Webb, R., Houser, P.: Development of a "Nature Run" for Observing System Simulation Experiments (OSSEs) for Snow Mission Development. Journal of Hydrometeorology 23, 351–375. https://doi.org/10.1175/JHM-D-21-0071.1, 2022.

Ying, Y.: Assimilating Observations with Spatially Correlated Errors Using a Serial Ensemble Filter with a Multiscale Approach. Monthly Weather Review 148, 3397–3412. https://doi.org/10.1175/MWR-D-19-0387.1, 2020.